Nanotechnology **13** (2002) 299–303 PII: S0957-4484(02)31405-3

Experimental and theoretical investigation of quantum point contacts for the validation of models for surface states

G Fiori[1], G Iannaccone[1], M Macucci[1], S Reitzenstein[2], S Kaiser[2], M Kesselring[2], L Worschech[2] and A Forchel[2]

[1] Dipartimento di Ingegneria dell'Informazione, Università degli studi di Pisa, Via Diotisalvi 2, I-56122 Pisa, Italy

[2] Technische Physik, Universität Würzburg, Am Hubland, D-97094 Würzburg, Germany

E-mail: g.fiori@iet.unipi.it

Received 30 November 2001, in final form 27 February 2002
Published 23 May 2002
Online at stacks.iop.org/Nano/13/299

Abstract

We have performed an investigation of quantum point contacts (QPCs) defined by split gates on AlGaAs/GaAs heterostructures in order to understand the effects of surface states on the transport characteristics of mesoscopic devices. We compare results from transport measurements on a large number of QPCs with simulations using a Poisson–Schrödinger solver in which the effects of surface states are taken into account. We show that surface properties strongly affect the conductance of QPCs, and that a simple model for surface states allows us to reproduce with reasonable accuracy the pinch-off voltage of QPCs with different gate layouts.

1. Introduction

Mesoscopic devices are typically defined by split gates or etching on modulation doped heterostructures. In order to obtain strong electron confinement and, consequently, to observe the transport properties typical of the mesoscopic regime at higher temperatures, the regions in which electron transport occurs must be very close to the surface.

In the case of devices defined electrostatically by metal gates evaporated on the semiconductor surface, stronger confinement is obtained if the heterointerface, where the two-dimensional electron gas (2DEG) is located, is at a small distance from the surface. On the other hand, this implies that surface properties strongly affect device behaviour.

From the point of view of fabrication, controlling the surface properties is crucial for the reproducibility of device characteristics. On the other hand, as far as device modelling is concerned, proper treatment of the surface is necessary to perform quantitatively accurate simulations.

In this paper, we investigate the effect of surface states on transport properties of quantum point contacts (QPCs), through experiments and simulations on the simplest devices exhibiting mesoscopic transport, i.e., QPCs defined by split gates on an AlGaAs/GaAs heterostructure.

We compare simulations performed with a purposely developed three-dimensional Poisson–Schrödinger solver with transport measurements, and show that results in quantitative agreement with the experiment can be obtained if a reasonable model for surface states is included in the simulations.

Surface states are usually treated with drastic approximations, such as Fermi level pinning or the assumption of a frozen charge at the air–semiconductor interface [1–3]. However, these approximations are unable to reproduce the experimental results [4,5]. In this paper, a slightly more complex model, typically used for metal–semiconductor contacts, is shown to be adequate for reproducing the experimental pinch-off voltages.

The experiments performed and the physical model considered are described in sections 2 and 3, respectively. In section 4 we present theoretical conductance–voltage characteristics, and compare results from experiments and simulations. We also evaluate quantitatively the dispersion of the pinch-off voltage of QPCs due to the discrete distribution of impurities in the doped layer. Section 5 concludes the paper.

0957-4484/02/030299+05$30.00 © 2002 IOP Publishing Ltd Printed in the UK

Cap layer 9nm GaAs

Doped layer (Si) 31 nm $Al_{0.2}Ga_{0.8}As$

Spacer 12 nm $Al_{0.2}Ga_{0.8}As$

500 nm GaAs

Figure 1. Layer structure of the AlGaAs/GaAs heterostructure on which the QPCs are defined.

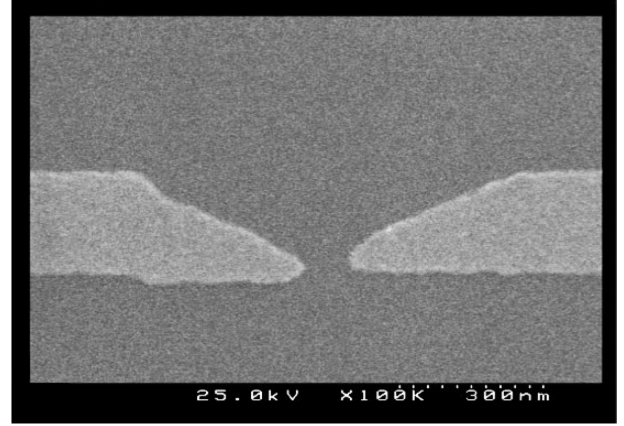

Figure 2. SEM picture of the gate layout of one of the considered QPCs with an actual lithographic gap of 112 nm.

2. Experiment

QPCs defined by split gates on AlGaAs/GaAs modulation doped heterostructures have been fabricated and characterized by means of transport measurements at 0.3 K. The samples were grown by molecular beam epitaxy, with the layer structure shown in figure 1, consisting of an undoped GaAs substrate, an undoped 12 nm spacer layer of $Al_{0.2}Ga_{0.8}As$, a 31 nm layer of doped GaAs (donor concentration $N_D \approx 10^{18}$ cm^{-3}), and an undoped 9 nm GaAs cap layer. The Hall mobility of the structure is 1×10^6 cm^2 V^{-1} s^{-1} with a carrier concentration of 3.7×10^{11} cm^{-2} at 4.2 K in the dark.

UV lithography was used to expose the Hall bar and the contact pads on top of the high mobility heterostructure. Wet etching was used to remove 200 nm and to separate electrically twelve single devices for each sample. In a second step, the contacts were realized by a contact mask and evaporation of Au/Ge/Ni layers followed by alloying. High resolution electron beam lithography at 100 kV was used to define masks for the split gates.

Three different gate layouts have been defined, corresponding to nominal lithographic gaps of 50, 100, and 150 nm, respectively. For each gate layout, several samples have been realized and characterized by standard lock-in techniques, in order to evaluate the dispersion of the transport characteristics of the QPCs. A SEM picture of the gate layout of a QPC with a nominal gap of 100 nm is shown in figure 2; the actual lithographic gap, measured from the SEM image, is 112 nm. For the simulations described in the following sections, we consider an 'actual' gate layout of the split gate structure, extracted from the SEM image, for each of the three nominal layouts considered.

Various structures exhibit conductance quantization at integer multiples of $2e^2/h$, as an indication of ballistic transport of electrons through a QPC defined by depletion of electrons beneath the metallic gates. For negative gate voltages exceeding the pinch-off voltage, the conductance increases until reaching a plateau at $2e^2/h$, which corresponds to the population of the first subband in the constriction. With increasing gate voltage, further subbands are occupied, which results in a step-like function of the conductance. The average pinch-off voltage and its standard deviation for the three gate layouts considered are reported in table 1.

3. Model

3.1. Poisson–Schrödinger solver in three dimensions

The potential profile in the three-dimensional structure obeys the Poisson equation

$$\nabla[\varepsilon(\vec{r})\nabla\phi(\vec{r})] = -q[p(\vec{r}) - n(\vec{r}) + N_D^+(\vec{r}) - N_A^-(\vec{r})], \quad (1)$$

where ϕ is the electrostatic potential, ε is the dielectric constant, p and n are the hole and electron densities, respectively, N_D^+ is the concentration of ionized donors and N_A^- is the concentration of ionized acceptors. While hole, acceptor and donor densities are computed in the whole domain with the semiclassical approximation, the electron concentration in the 2DEG is computed by solving the Schrödinger equation with density functional theory.

The observation that electron confinement is strong along the direction perpendicular to the AlGaAs/GaAs interface has led us to decouple the Schrödinger equation into a one-dimensional equation in the vertical (x) direction and a two-dimensional equation in the y–z plane; the density of states in the horizontal plane is well approximated by the semiclassical expression, since there is no in-plane confinement, while discretized states appear in the vertical direction. The single particle Schrödinger equation in three dimensions reads

$$-\frac{\hbar^2}{2}\frac{\partial}{\partial x}\frac{1}{m_x}\frac{\partial}{\partial x}\Psi - \frac{\hbar^2}{2}\frac{\partial}{\partial y}\frac{1}{m_y}\frac{\partial}{\partial y}\Psi - \frac{\hbar^2}{2}\frac{\partial}{\partial z}\frac{1}{m_z}\frac{\partial}{\partial z}\Psi + V\Psi = E\Psi; \quad (2)$$

we can write $\Psi(x, y, z)$ as $\Psi(x, y, z) = \psi(x, y, z)\chi(y, z)$. By substituting the above expression in (2) we obtain

$$-\frac{\hbar^2}{2}\chi\frac{\partial}{\partial x}\frac{1}{m_x}\frac{\partial}{\partial x}\psi - \left[\frac{\hbar^2}{2}\frac{\partial}{\partial y}\frac{1}{m_y}\frac{\partial}{\partial y} + \frac{\hbar^2}{2}\frac{\partial}{\partial z}\frac{1}{m_z}\frac{\partial}{\partial z}\right]\psi\chi + V\psi\chi = E\psi\chi, \quad (3)$$

Table 1. Experimental and theoretical values of the pinch-off voltage for several QPCs with three different nominal lithographic gaps.

Nominal gap (nm)	Actual gap a (nm)	Number of samples	Average V_P (experiments) (mV)	Standard deviation (experiments) (mV)	V_P (simulation) (mV)
50	57	14	−456	81	−465
100	112	4	−665	52	−656
150	140	4	−1219	61	−1198

where the dependence on x, y and z is omitted for clarity. If ψ satisfies the Schrödinger equation along the x-direction

$$-\frac{\hbar^2}{2}\frac{\partial}{\partial x}\frac{1}{m_x}\frac{\partial}{\partial x}\psi + V\psi = \tilde{E}(y,z)\psi, \tag{4}$$

and by substituting equation (4) into (3) we obtain

$$-\left[\frac{\hbar^2}{2}\frac{\partial}{\partial y}\frac{1}{m_y}\frac{\partial}{\partial y} + \frac{\hbar^2}{2}\frac{\partial}{\partial z}\frac{1}{m_z}\frac{\partial}{\partial z}\right]\psi\chi = E\psi\chi - \tilde{E}(y,z)\psi\chi. \tag{5}$$

Assuming that $\psi(x, y, z)$ is weakly dependent on y and z, and defining

$$\hat{T}_{yz} \equiv -\frac{\hbar^2}{2}\frac{\partial}{\partial y}\frac{1}{m_y}\frac{\partial}{\partial y} - \frac{\hbar^2}{2}\frac{\partial}{\partial z}\frac{1}{m_z}\frac{\partial}{\partial z}, \tag{6}$$

equation (5) can be approximated as

$$\psi\hat{T}_{yz}\chi = \psi[E - \tilde{E}_i(y,z)]\chi, \tag{7}$$

where $\tilde{E}_i$ is the ith eigenvalue of equation (4). Since $\tilde{E}_i(y, z)$ in the cases considered is rather smooth in y and z, we assume that the eigenvalues of equation (7) essentially obey the two-dimensional semiclassical density of states. The assumption is justified from a quantitative point of view in [7].

The confining potential V can be written as $V = E_C + V_{exc}$, where E_C is the conduction band and V_{exc} is the exchange–correlation potential within the local density approximation [8]

$$V_{exc} = -\frac{q^2}{4\pi^2\varepsilon_0\varepsilon_r}[3\pi^3 n(\vec{r})]^{\frac{1}{3}}. \tag{8}$$

For GaAs, we have $m_x = m_y = m_z = m = 0.067\,m_0$, where m_0 is the electron mass, therefore the electron density can be written as

$$n(x,y,z) = \frac{k_B T m}{\pi\hbar^2}\sum_{i=0}^{+\infty}|\psi_i(x,y,z)|^2 \ln \times\left[1 + \exp\left(-\frac{\tilde{E}_i(y,z) - E_F}{k_B T}\right)\right], \tag{9}$$

where ψ_i and $\tilde{E}_i$ are the eigenfunctions and eigenvalues of equation (4), respectively.

To solve self-consistently the Poisson–Schrödinger equation, we have used the Newton–Raphson method with a predictor/corrector algorithm close to that proposed in [6]. In particular, the Schrödinger equation is not solved at each Newton–Raphson iteration step. We assume that the shape of the eigenfunctions is not affected by variations of the potential and that the eigenvalues are only shifted by a quantity $q(\phi - \tilde{\phi})$, where $\tilde{\phi}$ is the potential used in the previous solution of the Schrödinger equation and ϕ is the potential at the current iteration. Within a Newton–Raphson cycle, the electron density reads

$$n(x,y,z) = \frac{k_B T m}{\pi\hbar^2}\sum_{i}|\psi_i(x,y,z)|^2 \ln \times\left[1 + \exp\left(-\frac{\tilde{E}_i(y,z) - E_F + q(\phi - \tilde{\phi})}{k_B T}\right)\right]. \tag{10}$$

When convergence is achieved the Schrödinger equation is solved again, and the new eigenfunctions are used in a new Newton–Raphson algorithm. Such a procedure is repeated until the norm of two consecutive solutions of the Newton–Raphson cycle is smaller than a predetermined value.

3.2. Surface states

Surface states can strongly influence the behaviour of devices defined on a 2DEG in proximity of the surface. We assume a model for surface states typically applied to metal–semiconductor interfaces [1] and based on two parameters—an effective work function Φ^* and a uniform density of surface states per unit area per unit energy D_s—that are properties of the semiconductor surface and depend on the fabrication process. The effective work function, as shown in figure 3, represents the difference between the Fermi level at the surface and the vacuum energy E_0 when the surface charge density is zero. We make the additional assumption that all the surface states below Φ^* behave as donors and all surface states above Φ^* behave as acceptors. The surface charge density due to surface states can therefore be expressed as

$$\rho_{ss} = qD_s[E_0 - \Phi^* - E_F] \tag{11}$$

where E_0 is the vacuum energy level. If we assume that surface states are very effective in shielding the electric field, so that the electric field in the air is zero, we can limit our simulation domain to the semiconductor region and apply the following boundary condition at the air–semiconductor interface

$$\vec{E}\cdot\vec{n} = q\frac{D_s}{\varepsilon}[E_0 - \Phi^* - E_F], \tag{12}$$

where $\vec{E}$ is the electric field in the semiconductor, and $\vec{n}$ is the unit vector normal to the semiconductor surface.

If $D_s \to \infty$, the Fermi level at the surface is pinned at the level $E_0 - \Phi^*$ and the surface practically behaves as a metallic layer with work function Φ^*.

The parameters of the surface state model and the concentration of donors in the doped layer have been extracted from measurements on purposely fabricated test structures [5]: $\Phi^* = 4.85$ eV, $D_S = 5\times10^{12}$ cm^{-2} eV^{-1}.

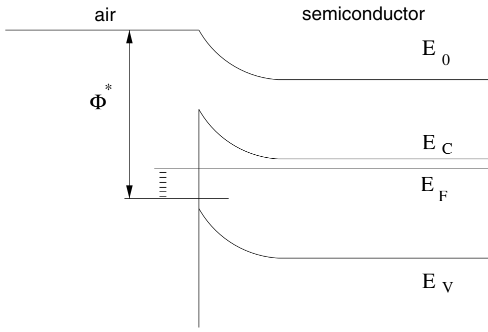

Figure 3. Sketch of the band profile at the air–semiconductor interface. Φ^* is the energy difference between the vacuum energy level E_0 and the Fermi level at the surface when the surface charge density is zero.

Table 2. Conductance simulated at different temperatures for a single QPC: $V_G = -0.45$ V.

Temperature	Conductance units of $2e^2/h$
100	2.36×10^{-10}
77	4.29×10^{-7}
50	5.6×10^{-4}
35	0.0132
25	0.065
20	0.118
15	0.186
10	0.254
5	0.299
4.2	0.299

4. Results

For our simulation, we have used the actual gate layout extracted from a SEM picture (for example, that shown in figure 2). Once the three-dimensional Poisson–Schrödinger equation is solved, we extract the first subband profile $\tilde{E}_1(y, z)$, which is the only populated subband, and compute the conductance of the QPC with a method based on recursive Green functions [9].

Convergence problems arise as the temperature is close to zero, because of the discontinuity of the Fermi–Dirac distribution. For this reason we have performed our simulations at the temperature of 4.2 K (measurements have been performed at 0.3 K). To achieve convergence at 4.2 K, we have to perform a 'cooling' procedure; we start with a simulation at 100 K, and progressively decrease the temperature down to 4.2 K. Actually, the conductance almost saturates when the temperature of 4.2 K is reached, as can also be seen in table 2. Therefore we reasonably compare the pinch-off voltages computed at 4.2 K with the experimental values at 0.3 K.

We have noticed that the pinch-off voltage is strongly dependent on the donor concentration in the doped layer N_D, which is known from experiments with insufficient accuracy. For this reason, we have considered N_D as a fitting parameter in order to reproduce the experimental pinch-off voltages of QPCs with different lithographic gaps. The best fit is provided by $N_D = 0.8 \times 10^{18}$ cm^{-3}. The electron concentration in the 2DEG is 4×10^{11} cm^{-2}, close to the experimental value.

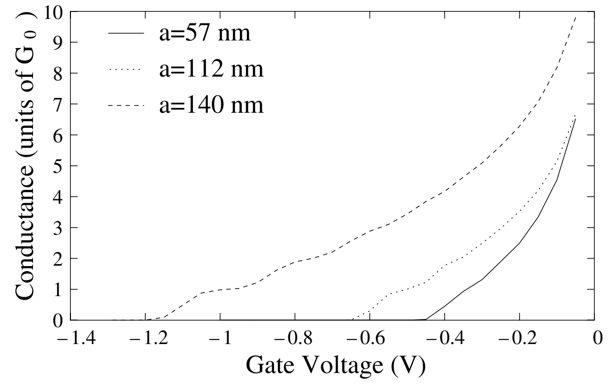

Figure 4. Simulated conductance as a function of gate voltage for devices with different 'actual' lithographic gaps.

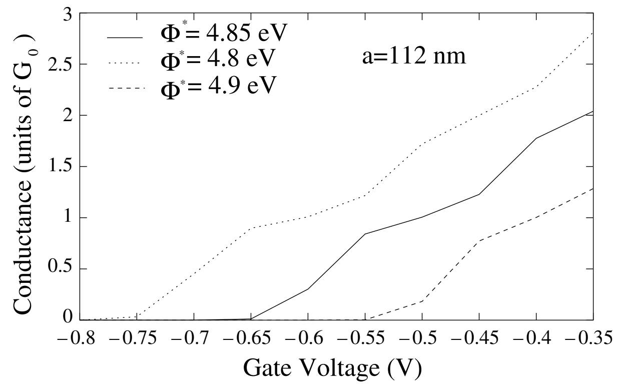

Figure 5. Simulated conductance as a function of gate voltage with varying Φ^* for the QPC with an actual lithographic gap of 112 nm.

In table 1 theoretical threshold voltages are compared with the experimental values, exhibiting a very good agreement. Theoretical G–V curves of QPCs with actual lithographic gaps of 57, 112 and 140 nm, corresponding to nominal gaps of 50, 100 and 150 nm, respectively, are shown in figure 4.

In order to investigate the dependence of conductance on the parameters of the model for surface states, we have computed the G–V curve for Φ^* ranging from 4.8 to 4.9 eV (figure 5) and D_S ranging from 2.5×10^{16} to 10^{17} m^{-2} eV^{-1} (figure 6). The pinch-off voltage depends significantly on both parameters; an accurate evaluation of their values is therefore mandatory to perform quantitative simulations of split gate structures.

We have performed a statistical simulation in order to assess from a quantitative point of view the effect of the random distribution of impurities in the doped layer on the dispersion of the G–V characteristics and of QPC pinch-off voltages. We assume that the number of impurities in each volume element of the grid obey a Poisson distribution. We can obtain an 'actual' distribution of dopants by considering, for each point of the grid k, its associated volume element ΔV_k and the nominal doping concentration N_{Dk}. The actual number of impurities in ΔV_k is obtained as a random number N'_k extracted with Poisson distribution of average $\Delta V_k N_{Dk}$. By dividing N'_k by ΔV_k we obtain the 'actual' local density of dopants.

We have then simulated an ensemble of sixteen geometrically identical QPCs (with $a = 57$ nm) with identical nominal doping profiles but different actual distributions of

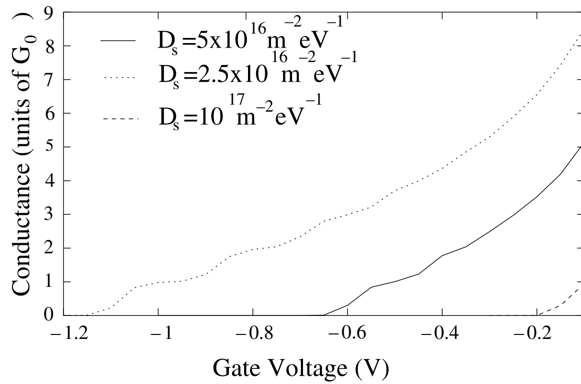

Figure 6. Simulated conductance as a function of gate voltage for D_s equal to 2.5×10^{16}, 5×10^{16} and 1×10^{17} m^{-2} eV^{-1}. The QPC considered has an actual lithographic gap of $a = 112$ nm.

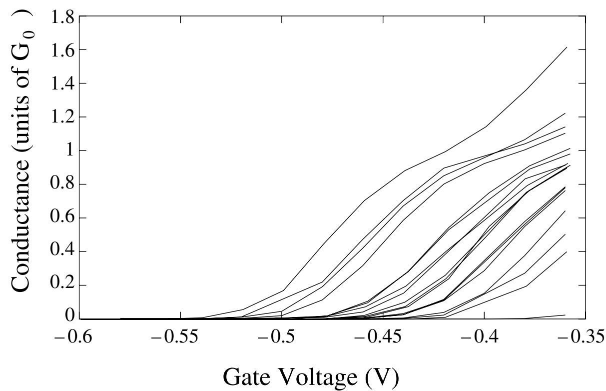

Figure 7. Simulated conductance as a function of the gate voltage for sixteen nominally identical QPCs with $a = 57$ nm, but different actual discrete dopant densities.

impurities and we have obtained a standard deviation of the pinch-off voltage $\sigma_{N_d} = 41.5$ mV. Simulated G–V curves of nominally identical QPCs with different 'actual' dopant distribution are shown in figure 7.

In the same way, we have taken into account the random distribution of surface states considering, for each point of the grid belonging to the exposed surface, the associated surface element ΔS. Figure 8 shows G–V curves derived from a random distribution of surface states. We have obtained a standard deviation of the pinch-off voltage due to discrete surface states $\sigma_s = 5.16$ mV. The total standard deviation of the pinch-off voltage is therefore $\sigma_T = \sqrt{\sigma_{N_d}^2 + \sigma_s^2} = 41.82$ mV, which is still smaller than the value of 81 mV obtained from experiments (shown in table 1). Such deviation may be due to other sources of dispersion, such as geometric tolerances.

5. Conclusions

A solver of the Poisson–Schrödinger equation in three dimensions has been developed, which includes a model for surface states based on two parameters: an 'effective' work function of the surface states and the density of surface states per unit area per unit energy. We have used an approximation

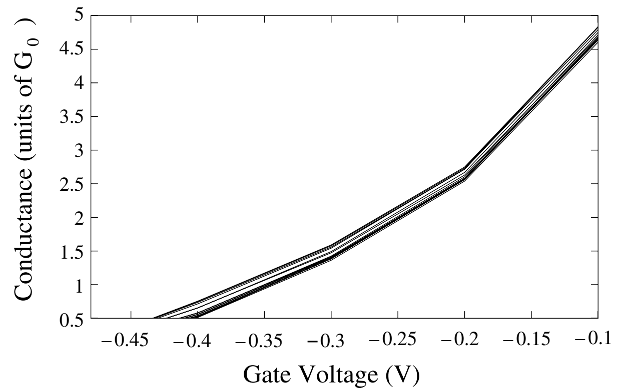

Figure 8. Simulated conductance as a function of gate voltage for twelve nominally identical QPCs with $a = 57$ nm, but different actual discrete surface state densities.

that allows us to solve the Schrödinger equation only in the vertical direction, with no practical loss of accuracy.

In order to validate the models used, several QPCs with different lithographic gaps have been realized on an AlGaAs/GaAs heterostructure and characterized from the electrical point of view in the regime of conductance quantization.

Pinch-off voltages obtained from experiments and simulation exhibit a very good agreement with just one fitting parameter, the donor concentration in the doped layer, which is usually known with insufficient precision to perform accurate simulations. Also, parameters of the density of surface states must be known with reasonable accuracy to perform simulations, and in our case they were independently obtained.

We have shown that our code can also include the effect of discrete impurities in the doped layer and of discrete surface states, and that such an effect accounts for about a half of the dispersion of pinch-off voltage measured in experiments, meaning that an additional source of dispersion, such as, probably, tolerance on the gate geometry, is predominant.

Acknowledgment

Support from the NANOTCAD project (IST 1999-10828 NANOTCAD) is gratefully acknowledged.

References

[1] Sze S 1981 *Physics of Semiconductor Devices* 2nd edn (New York: Wiley) pp 270–9
[2] Chen M and Porod W 1993 *J. Appl. Phys.* **75** 2545–54
[3] Davies J H and Larkin I A 1994 *Phys. Rev.* B **49** 4800–9
[4] Iannaccone G, Macucci M, Amirante E, Jin Y, Lanois H and Vieu C 2000 *Superlatt. Microstruct.* **27** 369–72
[5] Pala M, Iannaccone G, Kaiser S, Schliemann A, Worschech L and Forchel A 2002 *Nanotechnology* 373–7
[6] Trellakis A, Galick A T, Pacelli A and Ravaioli U 1997 *J. Appl. Phys.* **81** 7800–4
[7] Fiori G, Iannaccone G and Macucci M 2001 *Proc. 8th Int. Workshop on Computational Electronics* submitted
[8] Inkson J C 1986 *Many Body Theory of Solids—An Introduction* (New York: Plenum) pp 279–86
[9] Macucci M, Ravaioli U and Hess K 1989 *J. Appl. Phys.* **66** 3892–906